Composites Part B 112 (2017) 49–56

Contents lists available at ScienceDirect

Composites Part B

journal homepage: www.elsevier.com/locate/compositesb

Effect of tufting density and loop length on the crushing behaviour of tufted sandwich specimens

Jamie W. Hartley*, James Kratz, Carwyn Ward, Ivana K. Partridge

ACCIS, University of Bristol, Queen's Building, University Walk, Bristol BS8 1TR, UK

ARTICLE INFO

Article history:
Received 2 May 2016
Received in revised form
16 July 2016
Accepted 16 December 2016
Available online 19 December 2016

Keywords:
3-Dimensional reinforcement
Defects
Mechanical testing
Tufting

ABSTRACT

A series of small scale specimens were tested to identify if local variations during the manufacturing process influence the energy absorbed during the crushing of tufted sandwich structures. Coupons with varying loop lengths and number of tufts were tested in quasi-static and dynamic edgewise compression. Results of the testing showed that the effect of a single tuft was captured at this small scale, whilst the tufting parameters changed the damage behaviour, including the response of the resin column during testing. Increasing the number of tufts at a single point, from one to two or three, gave rise to a greater energy absorption, but variations in loop length were less conclusive.

1. Introduction

Energy absorbing structures must be able to maintain loads over prolonged crushing distances or to a targeted stopping fail-safe, using a minimal amount of material. Metallic structures absorb energy through a progressive folding mechanism, however this can prove difficult to manage over a short distance, such as during a vehicle side impact, and can require a complex system design. Continuous fibre composites, on the other hand, offer potential improvements in this situation over metals [1–4] through frictional losses at ply interfaces as well as the overall deformation of the structure [5].

In the case of composite sandwich structures this becomes more difficult to achieve, as the reinforced fibre skin tends to disbond from the core, resulting in a premature, catastrophic failure. To be able to absorb the large amount of energy required in a crash situation, composite sandwich structures must be able to fail in a stable end-crushing mode by fracture and splaying of the face sheets [6]. In order to ensure this happens, buckling and disbonding of the skins from the core must be avoided. Through-thickness reinforcement employing stitching and Z-pinning methods have been previously shown to successfully increase the adhesion between skin and core, stabilising skin disbonding, and containing failure [7–16]. These studies showed improvements across a range of load cases, including static compression, out-of-plane impact and edgewise crushing.

More recently, tufting has emerged as a popular method of localised Through-Thickness Reinforcement (TTR) for dry preforms. The tufting process involves inserting a single threaded needle through a preform, where friction within the preform is responsible for holding the thread in place as the needle is retracted. On the back face of the preform a loop of thread is formed. Dell'Anno et al. [17] recently published an in depth review of tufting technology and the manufacturing process, whilst Tan et al. have investigated the manufacture of tufted sandwich panels [18].

In terms of mechanical properties of tufted continuous carbon fibre reinforced laminates, Treiber [19] and Dell' Anno [20] have studied the effects of tufting and the tufting process in detail. They observed that tufting can significantly improve the delamination resistance (by threefold) within a laminate with only a small reduction (approximately 10%) in the in-plane mechanical properties due to the disruption of the tuft on the fibre alignment. Henao et al. [21,22] have also investigated the effect of tufting, focusing on how sandwich structures fail under 3-point bending, edgewise compression and out-of-plane impact. A combination of experimental and numerical techniques were employed to conclude that tufting can offer significant improvements to sandwich structures by restricting the disbonding of the face sheets [21], with an increase in energy absorption with increasing tuft densities during out-of-plane impact [22]. However, studies into the

* Corresponding author.
E-mail address: jh9799@bristol.ac.uk (J.W. Hartley).

http://dx.doi.org/10.1016/j.compositesb.2016.12.037

crushing performance of such materials are limited. In one study, Blok [23] focused directly on the use of tufted sandwich panels as energy absorbing structures. The author reported that tufted sandwich panels can improve energy absorption during an impact event, but the choice of core and skin materials will influence both the energy absorption and the net benefit of tufting a sandwich structure.

Despite these reported gains there is, as of yet, no real understanding of how variations within the manufacturing process may affect the performance of these structures under edgewise compression.

Even with the use of automated processing, variations in loop lengths within the same preform are still possible. Tight control of tuft formation is apparently reliant on the quality and consistency of the preform. The use of dry fabrics provides a number of opportunities for variation through ply slippage or incomplete consolidation. Any variations in thickness in the preform will change the distance the needle travels, resulting in possible variations of tuft length. The relatively low stiffness of the dry fabric and backing material will also allow the preform to bend as the needle is inserted, again changing its path and resulting in varying lengths of tufts. Upon inspecting a tufted preform, inconsistency in loop formation can be clearly seen (Fig. 1a), as well as seams lifting from the panel surface due to reduced tension in the thread (Fig. 1b).

The aim of this research was to investigate a method of testing local variations within tufted sandwich components, starting at the smallest possible level of a unit cell around a single tuft. The effect of variations in the tuft structure could be captured and characterised at this scale. For this investigation, the loop length and the number of tufts inserted at a single point were chosen as the design variables as these are directly controllable during the insertion process.

2. Material and methods

2.1. Coupon design

No standardised test methodology currently exists to test a single tuft out-of-plane, therefore the closest matching ASTM standard, C364 [24] (Edgewise Compression of Sandwich Structures), was adapted to suit the mechanical testing. A redesigned coupon geometry was required to promote a local crushing failure at the tip of the coupon. The newly proposed coupon geometry is comprised of three sections, as shown in Fig. 2. The base section consisted of a 15 mm × 15 mm square to clamp the coupon into an end support, similar to the ASTM standard. Clamping within the support stopped the specimen from slipping during the test but also restricted the skins from immediately disbonding from the

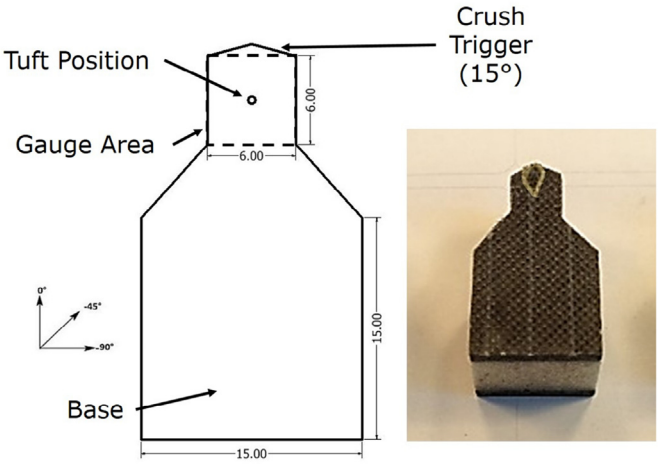

Fig. 2. Coupon geometry, **Left**: idealised, **Right**: actual.

core over the entire surface area. Some rotation was allowed at the base of the coupon and the upper crush plate was mounted to a spherical bearing to help align the specimen in the loading direction.

The gauge section of the coupon was a 6 mm × 6 mm square region, with the thread of the tuft located at the centre. The sizing for this was based around a 6 mm by 6 mm tuft spacing, which has been used in previously manufactured components [23].

Finally, to initiate crushing within the gauge section of the coupon, a taper to act as a crush trigger was included within the design. The trigger acted as a stress concentration to promote failure. The design intention was such that when contact occurred between the plate and the specimen at this sharp edge, the skins would begin to collapse, and crushing of the material would continue through the rest of the coupon. An angle of 15° was chosen for this design as this is above the threshold value for stable crushing [25].

2.2. Specimen manufacture

The sandwich panel used for testing was manufactured using the Vacuum-Assisted Resin Transfer Moulding (VARTM) technique. The preform was assembled using a uniweave carbon fibre fabric from SGL Automotive (300 g/m^2), and a 10 mm thick Rohacell® 110 IG-F closed-cell foam by Evonik (110 kg/m^3) for the core. The chosen layup was $[-45/0]_s$, giving a 2 mm thick skin. The preform was heated for 2 h at 90 °C under vacuum pressure to activate the binder in the carbon fabric before tufting using the robotic tufting

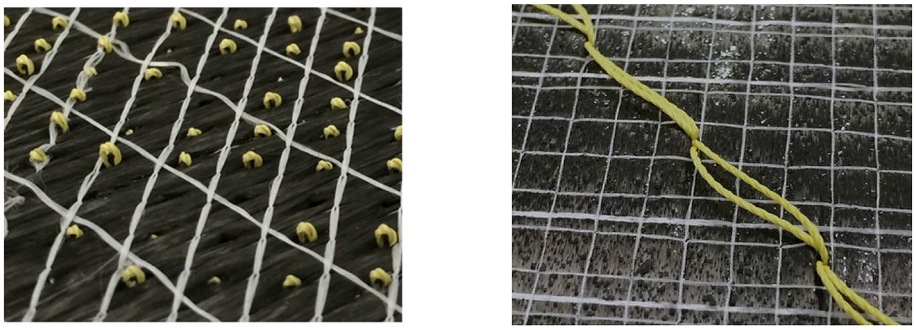

Fig. 1. Examples of observed variations in thread placement (representative only) **a)** variation in loop formation **b)** lifting of the thread from the preform surface.

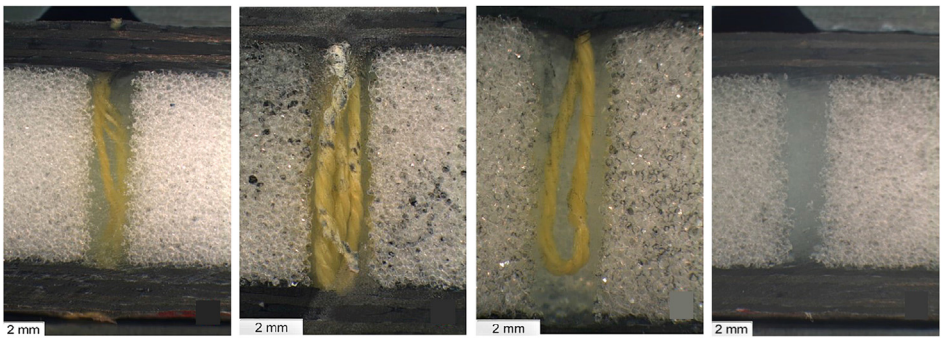

Fig. 3. Comparison of various tufting parameters.

unit at the UK National Composites Centre. A polystyrene backing sheet was placed below the preform to allow the needle to pass through the preform and form the loops on the backside. A nylon film was placed between the preform and the backing sheet to assist removal of the preform after tufting. The tufts were formed using a Tkt-20 Kevlar thread. The final tufted preform was then infused at 40 °C using EPIKOTE® Resin RIM 935 and EPIKURE® Curing Agent RIM 936 by Momentive. The cure cycle was two hours at 60 °C, one hour at 80 °C and a one hour post-cure at 90 °C. Test coupons were machined using a diamond saw, with a measured variation of ± 0.5 mm. The average coupon thickness was 14.8 mm, due to a resin rich layer formed at the surface around the tuft.

During the tufting process, the needle and presser foot starting positions were kept constant for every data series. The insertion rate (900 mm/min) and stitch length between tufts (15 mm) were also kept constant.

The input parameters were chosen to provide single tufts (Fig. 3a), with a range of loop sizes, defined as the length from the tip of the loop to the preform surface. In one seam, the needle was not fully inserted through the preform, resulting in a partial tuft that terminated within the core (Fig. 3c). In another, the thread was removed from the preform after tufting to leave a void within the panel that would completely fill with resin (Fig. 3d). To achieve a variation in local tuft density, double and triple tuft configurations were created by making multiple needle insertions at the same location. This process was chosen over reducing the tuft spacing as any reduction in spacing would lead to too significant a loss of the foam core and thus would have created an unstable panel. Increasing the thread thickness was also not possible due to the limitation of the needle eyelet and thread feed system. (Fig. 3b). A number of untufted baseline samples were also created. A summary of the tufting parameters used and the resulting loop sizes created for each sample series is shown in Table 1. As the diameter of the tufting needle (2 mm) is much greater than the Kevlar tufting thread (0.15 mm), a large void is formed within the foam core during tufting. During the infusion process, resin can freely flow into this void and fill it, resulting in large diameter columns of resin visible in the sandwich core.

After curing, the average loop size was measured by sampling 10 tufts within each seam, the results are shown in Table 1. As expected, reducing the needle penetration depth reduced the loop sizes formed; however, the loop formation was inconsistent, with significant variation of the loops sizes along each seam. This variation increases significantly with the insertion of multiple tufts, due to friction within the preform, as series 3 and 4 show the greatest standard deviation.

2.3. Static testing

Static testing was carried out using a Zwick 1466 test machine. Coupons were clamped into the end support and positioned at the centre of the loading plates. A displacement control program was used to provide a constant quasi-static crushing rate of 2 mm/min; chosen to replicate as close as possible the conditions outlined in ASTM C364 [24]. Fig. 4 shows the positioning of the specimen within the test machine. Testing was terminated after 10 mm of displacement as this ensured the entire tufted area had been crushed. A total of five samples were tested for each tuft configuration.

2.4. Dynamic testing

Dynamic testing was carried out using an Instron Dynatup 9250HV drop tower. Samples were mounted within the same support as for the static tests and impacted from above by an aluminium disk. Fig. 5 shows the set up for the dynamic testing. The

Table 1
Tufting parameters.

Series	No. of Tufts	Defined Material Depth (mm)	Needle Distance (mm)	Average Loop Size (mm)	SD	Average Mass (g)
1[a]	0	–	–	–	–	2.55
2	1	12	16	4.5	0.9	2.67
3	3	12	16	5.5	2.3	2.67
4	2	12	16	4.7	1.3	2.69
5	1	12	12	3.2	0.6	2.56
6	1	12	6	–	–	2.61
7	1	10	14	3.1	0.5	2.57
8	1	14	14	4	0.3	2.56
9[b]	0	14	14	–	–	2.59

[a] Baseline.
[b] Resin column (Fig. 3d).

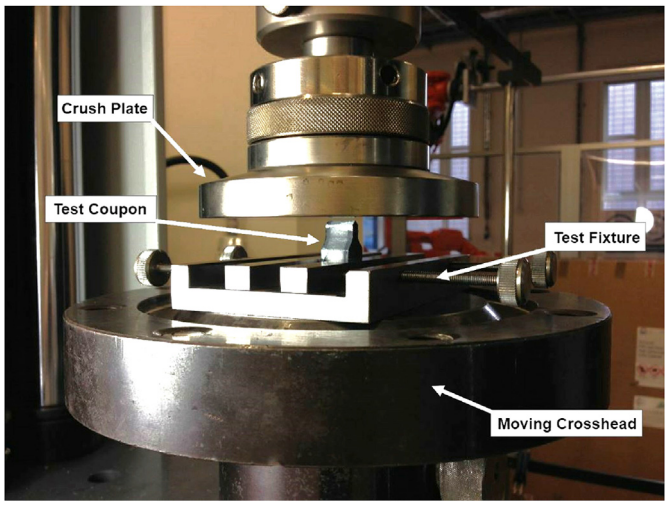

Fig. 4. Static test set-up.

selected impact energy was 20 J, chosen after an iterative process of increasing impact energies on additional test coupons to determine what energy level would progressively crush the entire gauge section. The impactor mass was 6.45 kg and the impact velocity was 2.5 m/s. A total of two samples were tested per tuft configuration.

2.5. Core removal

After testing, several samples of interest were selected for further inspection through removal of the foam core by dissolving in an alkaline solution. A sodium hydroxide solution of 30 wt% was mixed and the selected samples allowed to soak for several hours. To increase the rate of dissoloution, an ultrasonic water bath was used, heated to 50 °C. Removal of the foam core allowed inspection of the failure site to determine possible failure mechanisms.

3. Results and discussion

3.1. Static crushing

A tested specimen with a single tuft is shown in Fig. 6. The observed failure modes included progressive splaying and bending of the skins, delamination within the skins, and crushing of the foam core. From the top view only traces of the Kevlar thread are visible at the surface.

Representative load-displacement traces for several of the test configurations are compared in Fig. 7. The chosen curves have been selected for clarity, to illustrate the differences between the data series. From the graph it can be seen that each of the curves follows a distinctly similar trend that can be divided into four phases. In phase A, each of the curves show an approximately linear increase in load as the sandwich coupon resisted the applied crushing load. At its peak, the tapered trigger began to fracture and there was a noticeable drop in load. In phase B, crushing occurred within the gauge section of the coupon, with folding of the skins alongside compression of the foam core. It was at this point that, where present, the tuft begins to restrain the skins to the core, shown by an increase in the load applied to the coupon. In the selected curves shown in Fig. 7, there is a clear load recovery within the tufted coupons when compared to the untufted baseline and the sample with only a resin column. There is also some suggestion of a hierarchy, with the baseline and resin column samples showing the lowest performance, followed by an increasing load recovery observed in the partial tuft, standard single tuft, and then triple tufted samples. The lack of thread within the resin column appears to significantly reduce performance, resulting in a comparable or potentially weaker structure than the baseline sandwich. Surprisingly, the partially tufted coupon behaved similarly to the full insertion, single tuft specimen. In phase C, the load can be attributed to continual crushing of the remaining part of the gauge section after the tuft. In phase D, an increased crushing load of the baseline coupon was observed. This was due to densification of the foam core, but also because at this point the coupon geometry begins to widen. However, this was not observed in the other tufted

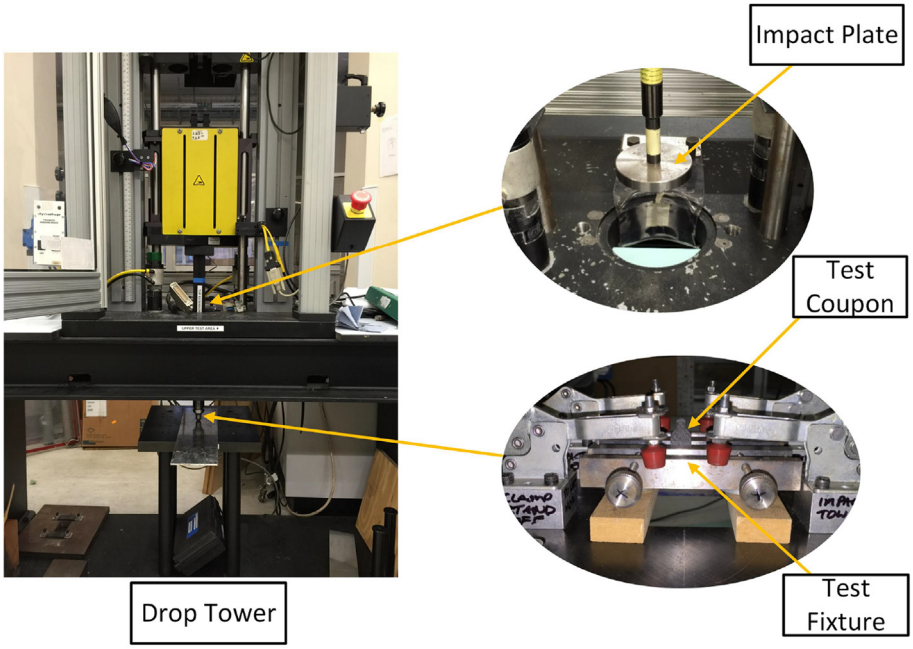

Fig. 5. Dynamic test set-up.

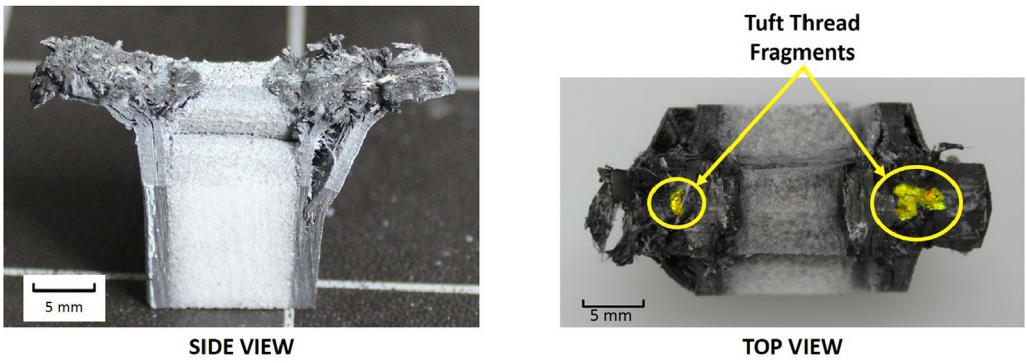

Fig. 6. Typical test failure mode (tuft fragments highlighted for clarity).

coupons, which remained constant through this region. In a number of the tufted samples, cracks between the skin and core propagated through to the base of the coupon, which appeared to delay core densification, and this could be the cause of the relative load reduction compared to the baseline. Tests were stopped at a crosshead displacement of 8 mm, to ensure the tuft effect in region B had been captured. Beyond this point there was inadequate clearance between the crush plate and the test fixture to continue testing.

Fig. 7 shows that the test method is able to capture the potentially positive effect of adding a tuft on the crushing performance of composite sandwich structures. The load recovery exhibited within the tufted specimens shows the desired reinforcement mechanism that counters the disbonding between the skins and core, but the additional load recovery shown by the baseline samples is not observed within any of the tufted samples. This suggests a further mechanism taking place after the failure of the tuft.

Fig. 8 shows several samples of interest after the core was removed. The samples represent four of the major tuft configurations; untufted, partially tufted, single tufted and triple tufted. Each of the columns shows some of the skin material remaining attached at each end. The degree of attached material appeared to vary between each sample, where the untufted interface has the least amount of material and the triple tuft interface has the most. This implies that the dominant failure mode of the tuft changes depending on how the thread is inserted or how many threads are used. Where no thread is present at the interface a clean break between skin and core was observed, but when the thread is present a fracturing of the surrounding skin takes place. Each of the tufted columns feature Kevlar tassels protruding from the skin, but at this time the mode of failure of the tuft thread is not clear.

This is an important observation, as the column remaining intact will allow it to displace through the core as crushing progresses. This mechanism could have a significant effect on the global failure of a tufted sandwich structure, as friction within the core could lead to additional energy absorption. However it could also have a negative effect as the movement of the column could force the skins away from the core and contribute to disbonding of the sandwich. This could explain why the baseline coupons show a second load recovery in section D, whilst the tufted ones do not.

3.2. Dynamic crushing

Fig. 9 shows representative load-displacement curves for the dynamic tests divided into the same four phases as the static tests (Fig. 7). Similarly to the static tests, an initial loading phase up to crush initiation was observed, followed by a load recovery due to the tuft, and finally a progressive crushing phase. Within phase B there is a clear distinction between those samples that are tufted and those that are not, with the triple tufted sample again sustaining the highest crushing load. It is noteworthy that within this section the single and partial tufted samples are more clearly

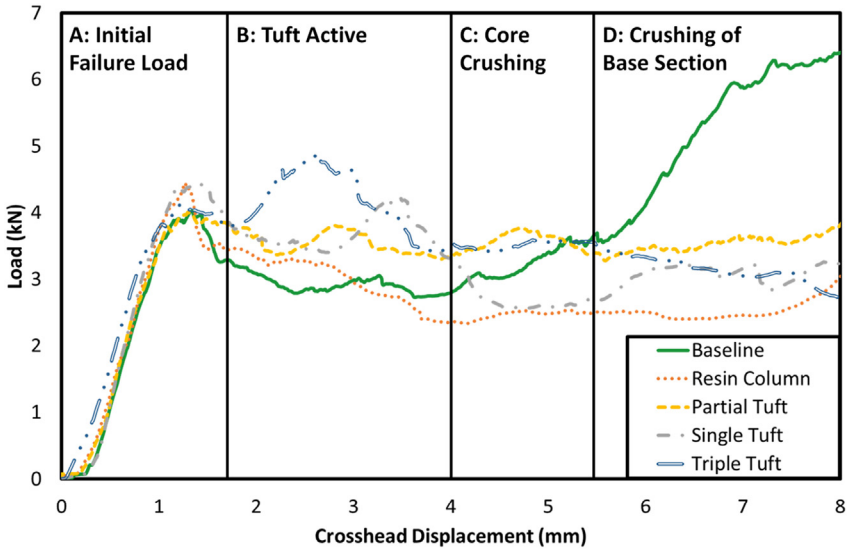

Fig. 7. Representative quasi-static load-displacement results.

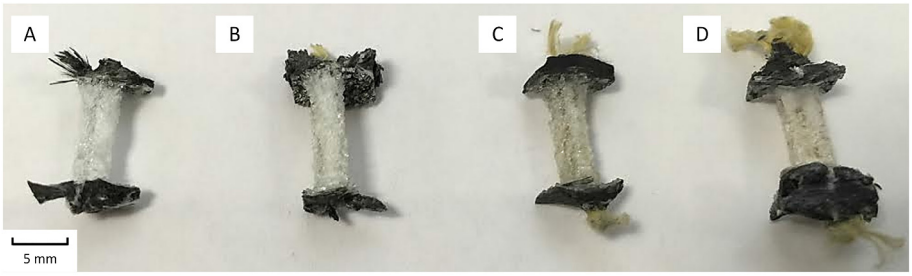

Fig. 8. Failed tuft columns, **A**: no thread, **B**: partial tuft, **C**: single tuft, **D**: triple tuft.

separated from the untufted samples than during the static testing. After phase B, the samples all converge to a similar level, except the baseline which undergoes a second load recovery as the sample geometry widens, as was observed in the static tests. Another observable trend is the termination point of the crushing failure, despite each sample being impacted with the same amount of energy. The triple tufted sample appears the most efficient as it stopped the impact in the shortest distance. This is followed by the single tufted sample, the baseline and then the partial tuft and resin column samples, which stopped at a similar point.

3.2.1. Energy absorption

A key metric for defining the capability of composite materials as energy absorbing devices is the Specific Energy Absorption (SEA). This value is based upon the load-displacement curve of the material under compression, which can be characterised by a peak force, attributed to the elastic properties of the structure prior to fracture, followed by a mean crushing force [5]. From this curve the SEA can be derived as in Equation (1):

$$SEA = \frac{W}{\rho A \delta} = \frac{\int_0^{\delta} F dx}{\rho A \delta} \quad (1)$$

where W is the work done on the structure during crushing (force x displacement), and $\rho A \delta$ defines the mass of the crushed material. The specific energy was approximated by integrating the area under the averaged load-displacement curve using the trapezium rule and then dividing by the crushed mass of the coupon, as in Equation (1). To approximate the mass of the crushed material, an average sandwich density was approximated by using the surface area of the test coupons using the dimensions shown in Fig. 2 and dividing by the coupon mass to give an approximate areal density of the coupon. By calculating the surface area of the coupon over the chosen crushing distance, the material density could then be used to find the crushed material mass.

To be able to isolate the region in which the tuft is active, and thus directly compare each configuration, the summation of the energy absorption and subsequent crushed mass was only carried out over the first 4.5 mm of crosshead displacement (Fig. 7). The calculated energy absorption values for both static and dynamic tests are shown in Fig. 10.

Although the values may be artificially inflated by the scale of the test coupon used, the results of the energy absorption analysis further support the variation in behaviour of the different tufting configurations. For both test types, these can be collected together into three distinct groups. The lowest performing coupons were the baseline and resin column samples. The second group contains the single tufted samples of varying loop lengths, including the partially tufted coupons. There is an increase over the baseline tests, however there is no clear trend within this group between the loop size and the resulting energy absorption. The final group contains the multiple thread tufted coupons, which show a clear jump over the baseline and single tufted specimens. For the static SEA results a one-way ANOVA analysis was carried out using the Holm-Sidak method and a significance level test of 0.05 in order to

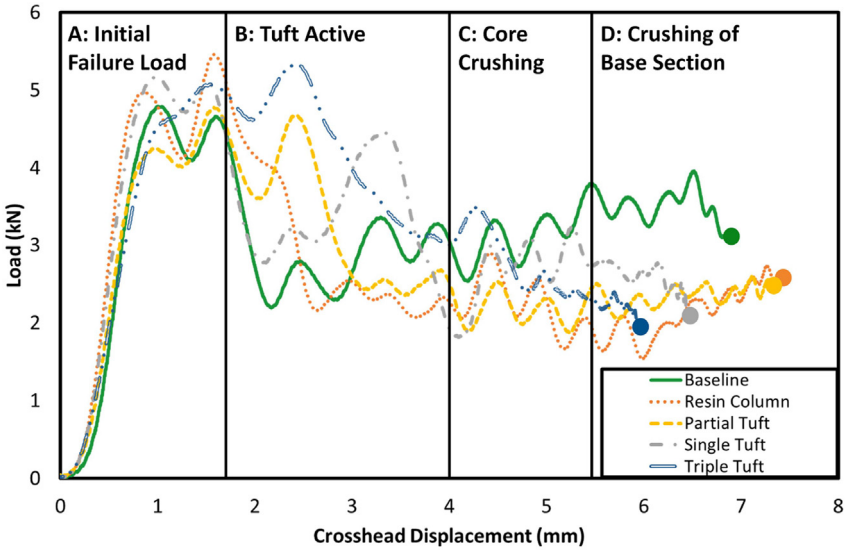

Fig. 9. Representative dynamic load-displacement results.

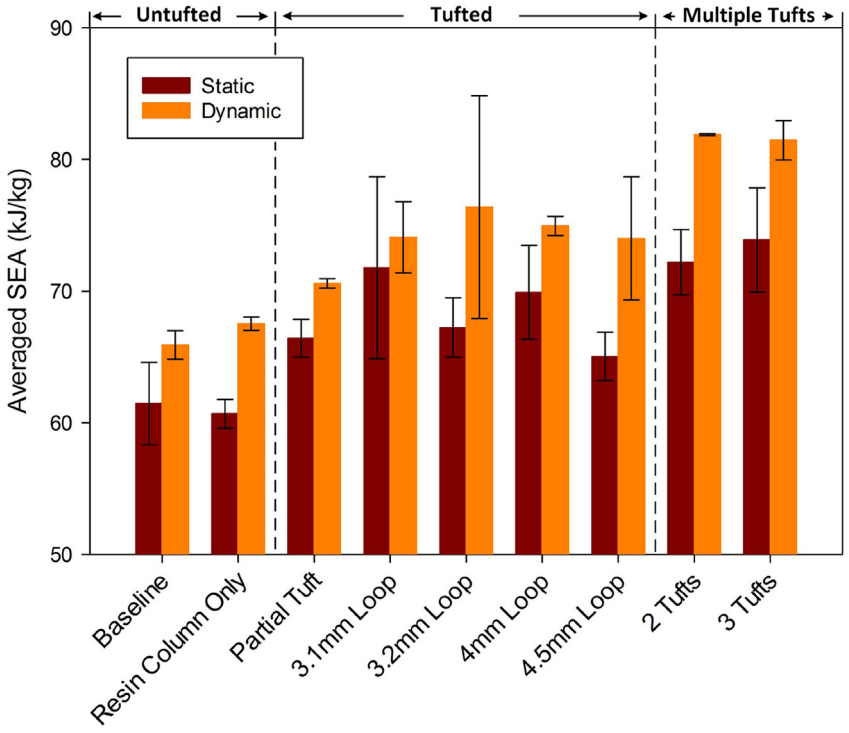

Fig. 10. Averaged SEA results for static and dynamic tests.

identify if a statistically significant difference could be observed in the test data. This analysis showed that the difference between several of the single and multiple tuft samples, and the untufted baseline samples were statistically significant. It also highlighted that the difference between those of varying loop size did not show a significant change. The dynamic test results appear to show a slight increase in energy absorption over the static tests, although the deviation of the results is generally high due to the small number of samples tested and this meant it was not possible to carry out an ANOVA analysis.

Analysing the energy absorbed during crushing shows that it is difficult to quantify the effect of loop length. Each series shows an increase over the baseline, but between these series a trend is not clear. It should be noted that the loop lengths with the highest performance also had the most significant variation. This is potentially an effect of the loop direction at the surface of the coupon. Due to the limited size of the gauge area, a coupon not aligned correctly may be cut short during machining and have its performance affected. It is also still not clear how the thread itself is behaving, as was shown in Fig. 8, where thread pull-through is not clear. The highest performing were the multiple tuft samples, which is unsurprising as Fig. 8 appears to show a greater amount of surrounding material around the tuft fractures during failure. It is likely for this reason that loop length does not have as significant an influence on performance.

Despite the lack of a clear trend between loop length and performance, several other potentially important observations were made. The comparative performance of both the partial and fully inserted tuft coupons is a promising sign for creating a potentially lighter (through shorter resin column) structure, with a cleaner surface finish. The use of multiple tuft insertions was shown to improve energy absorption and could lead to a high performing structure. Finally the observation of the column failure type and the subsequent displacement could have a significant effect on the global failure of a tufted structure, and needs to be investigated further to understand what influence it has.

4. Conclusion

A mechanical testing process has been used to demonstrate that the behaviour of individual tufts under both quasi-static and dynamic edgewise compression. Comparing the load-displacement results, a clear load recovery during the crushing of the tufted coupons was observed, which was not present in the untufted coupons. This implies that the tuft is counteracting the peeling mechanism of the skins and thus increasing the crush strength of the material between 11 and 19%. Modifying the length of the tuft appeared to have a negligible effect on the loading response with no clear trend between loop size and the amount of energy absorbed. This is an encouraging sign for process robustness during tufting sandwich structures. However, increasing the number of tufts within a sample did significantly increase the crushing performance by as much as 25%, when compared to the untufted coupons. Individual tufts and the surrounding resin column remained intact after testing, with an apparent increased failure site observed at the interface between skin and core when using multiple tufts, implying a change in the failure mode. Displacement of the tuft through the structure could have a significant effect on the crushing behaviour and thus would need to be studied in the future.

Acknowledgements

This work was supported by the Engineering and Physical Sciences Research Council through the EPSRC Centre for Doctoral Training in Advanced Composites for Innovation and Science (Grant: EP/G036772/1) and the EPSRC Centre for Innovative Manufacturing in Composites (CIMComp) (Grant: EP/IO33513/1). The authors would also like to acknowledge the contributions of Harry Clegg (NCC) and Paul Berry (UoB) for their assistance in the manufacture of the test coupons.

References

[1] Thornton P. Energy absorption in composite structures. J Compos Mater 1979;13(3):247–62. http://dx.doi.org/10.1177/002199837901300308.

[2] Carruthers J, Kettle A, Robinson A. Energy absorption capability and crashworthiness of composite material structures: a review. Appl Mech Rev 1998;51(10):635. http://dx.doi.org/10.1115/1.3100758.

[3] Jacob G, Fellers J, Simunovic S, Starbuck J. Energy absorption in polymer composite materials for automotive crashworthiness. J Compos Mater 2002;36(7):813–50. http://dx.doi.org/10.1177/0021998302036007164.

[4] Jacob G, Starbuck J, Fellers J, Simunovic S. Energy absorption in chopped carbon fiber epoxy composites for automotive crashworthiness. Polym J 2003;35(7):560–7. http://dx.doi.org/10.1295/polymj.35.560.

[5] Lukaszewicz DHJ. Advanced composite materials for automotive applications. Chichester, UK: John Wiley & Sons Ltd; 2013, ISBN 9781118535288. http://dx.doi.org/10.1002/9781118535288.

[6] Mamalis A, Manolakos D, Ioannidis M, Papapostolou D. On the crushing response of composite sandwich panels subjected to edgewise compression: experimental. Compos Struct 2005;71(2):246–57. http://dx.doi.org/10.1016/j.compstruct.2004.10.006.

[7] Raju K, Tomblin J. Energy absorption characteristics of stitched composite sandwich panels. J Compos Mater 1999;33(8):712–28. http://dx.doi.org/10.1177/002199839903300804.

[8] Potluri P, Kusak E, Reddy T. Novel stitch-bonded sandwich composite structures. Compos Struct 2003;59(2):251–9. http://dx.doi.org/10.1016/S0263-8223(02)00087-9.

[9] Sharma S, Krishna M, Murthy HN. Buckling response of stitched polyurethane foam composite sandwich structures. J Reinf Plast Compos 2004;23:1267–77. http://dx.doi.org/10.1177/0731684404037042.

[10] Marasco AI, Cartié D, Partridge IK, Rezai A. Mechanical properties balance in novel Z-pinned sandwich panels: out-of-plane properties. Compos Part A Appl Sci Manuf 2006;37:295–302. http://dx.doi.org/10.1016/j.compositesa.2005.03.029.

[11] Lascoup B, Aboura Z, Khellil K, Benzeggagh M. On the mechanical effect of stitch addition in sandwich panel. Compos Sci Technol 2006;66:1385–98. http://dx.doi.org/10.1016/j.compscitech.2005.09.005.

[12] Reis EM, Rizkalla SH. Material characteristics of 3-D FRP sandwich panels. Constr Build Mater 2008;22:1009–18. http://dx.doi.org/10.1016/j.conbuildmat.2007.03.023.

[13] Baral N, Cartié D, Partridge I, Baley C, Davies P. Improved impact performance of marine sandwich panels using through-thickness reinforcement: experimental results. Compos Part B Eng 2010;41(2):117–23. http://dx.doi.org/10.1016/j.compositesb.2009.12.002.

[14] Stapleton SE, Adams DO. Structural enhancements for increased energy absorption in composite sandwich structures. J Sandw Struct Mater 2010;13(2):137–58. http://dx.doi.org/10.1177/1099636210378951.

[15] Aktas A, Potluri P, Porat I. Development of through-thickness reinforcement in advanced composites incorporating rigid cellular foams. Appl Compos Mater 2012;20(4):553–68. http://dx.doi.org/10.1007/s10443-012-9285-4.

[16] Nanayakkara A, Feih S, Mouritz A. Experimental impact damage study of a z-pinned foam core sandwich composite. J Sandw Struct Mater 2012;14(4):469–86. http://dx.doi.org/10.1177/1099636212443915.

[17] DellAnno G, Treiber J, Partridge I. Manufacturing of composite parts reinforced through-thickness by tufting. Robotics Computer-Integrated Manuf 2016;37:262–72. http://dx.doi.org/10.1016/j.rcim.2015.04.004.

[18] Tan G, Hartley J, Withers E, Kratz J, Ward C. Towards the development of an instrumented test bed for tufting visualisation. SAMPE Eur Conf Amiens 2015. https://sampe.site-ym.com/store/ViewProduct.aspx?id=5380083.

[19] Treiber J. Performance of tufted carbon fibre/epoxy composites. Ph.D. thesis. Cranfield University; 2011. URL, https://dspace.lib.cranfield.ac.uk/handle/1826/5531.

[20] Dell'Anno G. Effect of tufting on the mechanical behaviour of carbon fabric/epoxy composites. Ph.D. thesis. Cranfield University; 2007. URL, https://dspace.lib.cranfield.ac.uk/handle/1826/2608.

[21] Henao A, Carrera M, Miravete A, Castejón L. Mechanical performance of through-thickness tufted sandwich structures. Compos Struct 2010;92(9):2052–9. http://dx.doi.org/10.1016/j.compstruct.2009.11.005.

[22] Henao A, de Villoria G, Cuartero J, Roberto, Carrera M, Pic\ón J, et al. Enhanced impact energy absorption characteristics of sandwich composites through tufting. Mech Adv Mater Struct 2015;22:1016–23. http://dx.doi.org/10.1080/15376494.2014.918221.

[23] Blok L. Testing and simulation of CFRP sandwiches with and without z- reinforcements during impact. 2014. Master's thesis; TU Delft.

[24] ASTM C364. Standard test method for edgewise compressive strength of sandwich constructions. 2014. http://dx.doi.org/10.1520/C0364.

[25] Velecela O, Soutis C. Prediction of crushing morphology of GRP composite sandwich panels under edgewise compression. Compos Part B Eng 2007;38(7–8):914–23. http://dx.doi.org/10.1016/j.compositesb.2006.11.001.